EAI Endorsed Transactions
on Energy Web

Research Article **EAI.EU**

Research on Target Recognition and 3D Reconstruction Technology for Distribution Network Patrol Based on BeiDou and Edge Computing

Ying Xie[1*], Yi Jiang[2], Lichao Cui[3], Yongjian Zhang [1], Jiangning Zhao[2]

[1]Department of Science, Technology and Digitalization, State Grid Zhejiang Electric Power Co., Ltd. Shaoxing Power Supply Company, Shaoxing 312000, Zhejiang Province, China
[2]Daxing Branch of Shaoxing Daming Electric Power Construction Co., Ltd., Shaoxing 312000, Zhejiang Province, China
[3]Yuecheng Branch, State Grid Zhejiang Electric Power Co., Ltd. Shaoxing Power Supply Company, Shaoxing 312000, Zhejiang Province, P.R. China

Abstract

INTRODUCTION: Power transmission and distribution lines operate in complex natural and electromagnetic environments, making them susceptible to risks such as tree encroachment, ice accumulation, insulator damage, and foreign object interference. Traditional inspection methods, including manual patrols and helicopter surveys, are inefficient, costly, and unsafe, and they lack real-time monitoring and large-scale coverage capabilities.
OBJECTIVES: This study aims to improve the accuracy, reliability, and real-time capability of distribution network inspections by developing an integrated target recognition and 3D reconstruction system based on BeiDou satellite communication and edge computing.
METHODS: An enhanced YOLOv8n-based target detection model incorporating C2f modules, lightweight convolution, and CBAM attention mechanisms is designed for real-time component and obstacle recognition. Point cloud clustering and graph embedding techniques are employed to reconstruct the three-dimensional structure of transmission lines and locate obstacles spatially. BeiDou short message communication is utilized to ensure stable data transmission under strong electromagnetic interference.
RESULTS: Experimental results show that the proposed system achieves superior performance in terms of mAP, F1 score, and small-object detection compared with baseline models. The system maintains stable communication in high-electromagnetic-interference environments and enables accurate 3D reconstruction and real-time fault perception across complex inspection scenarios.
CONCLUSION: The proposed BeiDou- and edge-computing-based inspection system effectively overcomes the limitations of traditional methods, significantly enhancing detection accuracy, communication reliability, and spatial perception for distribution network patrols, thereby improving grid safety and operational efficiency.

Keywords: BeiDou satellite communication; edge computing; YOLOv8; point cloud 3D reconstruction; power transmission and distribution inspection; unmanned aerial vehicle

Received on 08 January 2026, accepted on 11 July 2026, published on 21 September 2026

doi: 10.4108/ew.11534

[*]Corresponding author. Email: 13777332871@163.com

1. Introduction

With the continuous growth of global energy demand and the ongoing expansion of power system structures, the safe and stable operation of transmission and distribution networks has become a critical safeguard for national power infrastructure development and the normal functioning of modern industrial society [1,2]. Transmission and distribution lines are perpetually exposed to outdoor environments, facing potential risks from various natural and human factors, including tree encroachment, foreign object entanglement, icing faults, insulator damage, and bird nest accumulation [3]. If not promptly detected and addressed, these issues may trigger circuit tripping, insulation breakdown, partial discharge, or even widespread power outages, severely compromising supply reliability and system security. Therefore, achieving high-precision real-time inspection and intelligent risk early warning for transmission and distribution lines holds significant practical importance for enhancing grid dispatch capabilities, optimizing power operation and maintenance systems, and building intelligent energy systems [4,5]. This work addresses three critical gaps in intelligent power line inspection: poor communication in remote environments, separation of 2D detection from 3D reconstruction, and unreliable communication under high-voltage electromagnetic interference. The manuscript bridges these gaps by integrating BeiDou satellite communication, edge computing, and LiDAR-based 3D reconstruction into a unified system, benefiting utility companies and researchers developing UAV-based infrastructure inspection.

Traditional power line inspection methods primarily rely on manual periodic patrols or auxiliary technologies such as ground-based telescopes and helicopter aerial photography. However, manual inspections suffer from issues including enormous workload, high risk, low efficiency, and lack of real-time capability [6]. Helicopter inspections are costly, lack mobility, and are unsuitable for complex terrain areas. Fixed monitoring using tower-mounted cameras is limited by field-of-view constraints and installation conditions, making it difficult to cover long-distance distribution network lines. Consequently, unmanned aerial vehicle (UAV) inspections have gained significant attention in recent years as a key technology for intelligent power operation and maintenance, leveraging advantages such as flexibility, low cost, and high efficiency. However, practical UAV inspections still face critical challenges: First, visual imaging quality in complex environments is susceptible to factors like haze, backlighting, and obstructions, making it difficult for traditional image processing algorithms to accurately identify slender, densely packed conductors and accessory structures. Second, the significant size variation of targets in transmission and distribution line scenarios limits small object detection performance due to constraints in multi-scale feature representation capabilities [7,8]. Third, inspection areas such as mountainous and forested regions often experience weak or completely absent communication signals, making video and data transmission via public networks or single links unstable. Fourth, two-dimensional visual inspection struggles to support spatial geometric relationship analysis and precise position measurement, making the realization of three-dimensional scene understanding an urgent problem requiring breakthroughs.

To enhance the intelligence of inspection operations, scholars have conducted extensive research on deep learning-based target detection for transmission and distribution lines in recent years. For instance, [9] proposed applying YOLOv5 to small target recognition, improving the localization accuracy of line components in remote sensing images; [10] introduced deep convolutional networks for defect classification, partially alleviating the reliance of traditional image algorithms on manually defined features. Some studies have incorporated attention mechanisms and feature fusion strategies into transmission line scenarios, improving target discrimination capabilities in complex backgrounds. However, existing research still exhibits the following shortcomings: 1) Most methods are designed for single visual channels, relying solely on two-dimensional images for detection, making it difficult to ensure detection reliability in multi-interference environments; 2) There remains significant room for improvement in the recognition accuracy of small targets, slender structures, and densely arranged objects; 3) Research lacks comprehensive end-to-end approaches for inspection tasks, with insufficient integration of critical modules such as real-time communication, location awareness, and 3D spatial analysis; 4) Most models exhibit high computational complexity, making them unsuitable for deployment on UAV platforms and limiting real-time inspection capabilities.

To address the aforementioned challenges, this paper proposes a research framework for target recognition and 3D reconstruction in distribution network inspection scenarios, integrating BeiDou satellite communication with edge computing. Utilizing drones as mobile sensing and computing platforms, the framework employs optical cameras and LiDAR to collect multimodal inspection data. By deploying the improved YOLOv8n deep detection model on an edge computing platform, it enables real-time detection of critical components and potential risk targets along power transmission and distribution lines. To address communication disruptions in complex electromagnetic environments, such as mountainous and forested areas that prevent inspection data transmission, this study incorporates a BeiDou short message communication link. This enables highly reliable emergency data transfer, enhancing the continuity and safety of UAV inspection missions. The novelty of this work lies in an integrated UAV-based inspection framework that combines improved deep learning detection, 3D spatial reconstruction, and BeiDou satellite communication. Unlike existing approaches that treat these components separately, the proposed method enables system-level coordination with a lightweight design for real-time and practical UAV deployment.

The main contributions of this study are summarized as follows:

(1) An improved YOLOv8n-based target detection framework is developed for transmission and distribution network inspection by integrating the Convolutional Block Attention Module (CBAM), thereby enhancing feature

representation capability and improving the recognition accuracy of small targets, slender structures, and complex background objects.
(2) A lightweight convolution (Light Conv) module is introduced to reduce computational complexity and model parameters, thereby improving real-time inference efficiency and enabling practical deployment on UAV edge computing platforms.
(3) A BeiDou satellite communication linkage mechanism based on short message transmission is designed to ensure stable and reliable inspection data communication under weak-signal, mountainous, forested, and strong electromagnetic interference environments.
(4) A three-dimensional point cloud reconstruction and obstacle localization framework based on LiDAR data, clustering, and graph embedding techniques is proposed to achieve accurate spatial perception, obstacle localization, and geometric reconstruction of transmission and distribution network inspection environments.

2. Communication for Distribution Network Inspection in the BeiDou System

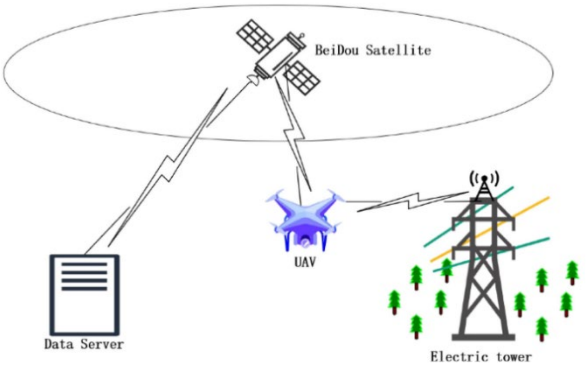

Figure 1. Design of a Communication and Positioning System for Distribution Network Inspection Based on BeiDou

Figure 1 illustrates the proposed intelligent distribution network inspection communication architecture based on the BeiDou Navigation Satellite System (BDS). This system integrates UAV inspection nodes, BeiDou satellite links, ground data servers, and the on-site environment of transmission and distribution lines, forming an "air-space-ground integrated inspection communication and perception closed-loop." During distribution line inspection tasks, the UAVs equipped with electro-optical cameras and 3D LiDAR capture environmental data around transmission towers. An embedded edge computing platform executes YOLO object detection and 3D point cloud modeling algorithms to enable real-time on-site recognition and obstacle location mapping. Simultaneously, to address weak or absent communication signals in mountainous and forested areas, the UAV transmits critical inspection data—including coordinate information, alarm statuses, and target recognition results—to ground servers in real time via Beidou short message links. This ensures continuous controllability and closed-loop task capability throughout the inspection process.
Regarding the positioning mechanism, this paper employs a BeiDou RNSS positioning model based on pseudorange measurements. The pseudorange between satellites and the UAV is quantified as:

$$\rho_i = c(t_r - t_s) \qquad (1)$$

A more precise pseudo-range expression is:

$$\rho_i = \sqrt{(x-x_i)^2 + (y-y_i)^2 + (z-z_i)^2} + c\delta t + \varepsilon_i \qquad (2)$$

where $\rho_i$represents the pseudorange measurement of the $i$the satellite, x, y, zdenotes the unknown position of the UAV, x_i, y_i, z_iindicates the satellite's spatial coordinates, (c) is the speed of light, $\delta t$is the receiver clock offset, and ε_i accounts for atmospheric refraction and multipath errors. Simultaneous measurements from at least four satellites form the following system of equations:

$$\begin{aligned}
\rho_1 &= \sqrt{(x-x_1)^2 + (y-y_1)^2 + (z-z_1)^2} + c\delta t + \varepsilon_1 \\
\rho_2 &= \sqrt{(x-x_2)^2 + (y-y_2)^2 + (z-z_2)^2} + c\delta t + \varepsilon_2 \\
\rho_3 &= \sqrt{(x-x_3)^2 + (y-y_3)^2 + (z-z_3)^2} + c\delta t + \varepsilon_3 \\
\rho_4 &= \sqrt{(x-x_4)^2 + (y-y_4)^2 + (z-z_4)^2} + c\delta t + \varepsilon_4
\end{aligned} \qquad (3)$$

The calculation yields the drone's three-dimensional spatial coordinates, achieving centimeter-level positioning accuracy. This provides a reliable foundation for subsequent three-dimensional point cloud spatial reconstruction and obstacle position calibration.
To ensure stable positioning during UAV motion, BeiDou pseudo range outputs are fused with IMU-based pose information (pitch, roll, and yaw) to compensate for motion-induced deviations. A filtering strategy is applied to suppress vibration and environmental noise, improving coordinate stability and real-time positioning accuracy in dynamic flight conditions.
Simultaneously, to ensure communication quality for critical alarm information during inspections, this paper employs the BeiDou RDSS short message protocol to construct the data frame structure. The short message data structure is defined as follows:

$$M = H \parallel ID \parallel P \parallel T \parallel D \parallel CRC \qquad (4)$$

Where H denotes the frame header identifier 0xBD, ID represents the device identification field, (P) indicates the packet number, (T) signifies the priority category field, (D) contains the payload data, and (CRC) stands for the checksum. The end-to-end communication reliability model for short messages is expressed as:

$$P_{succ} = 1 - (P_{loss})^N \quad (5)$$

P_{loss} represents the packet loss rate per transmission, and (N) denotes the number of retransmissions. Experimental results demonstrate that the system maintains a short message delivery rate exceeding 95% even under severe signal loss conditions, significantly outperforming inspection methods reliant on 4G/5G public networks.

Table 1. Comparison of BeiDou Communication and Traditional 4G/5G Networks for Distribution Network Inspection

Parameter	**BeiDou Communication**	**Traditional 4G/5G Networks**
Coverage in Remote Inspection Environments	Wide-area coverage suitable for mountainous, forested, and weak-signal regions	Dependent on cellular infrastructure and network availability
Latency Characteristics	Moderate latency suitable for inspection communication and emergency transmission	Lower latency, especially in 5G-enabled environments
Reliability Under Electromagnetic Conditions	More stable communication and positioning performance near power facilities	Signal quality may vary under strong electromagnetic interference
Suitability for Distribution Network Inspection	More suitable for remote and complex inspection environments	More effective in urban and network-covered areas

Compared with traditional 4G/5G networks, BeiDou communication provides broader coverage and more reliable communication in remote inspection environments and under varying electromagnetic conditions, as presented in Table 1. Although 4G/5G networks generally offer lower latency for real-time communication, BeiDou communication improves the reliability and practical applicability of UAV-based distribution network inspection in weak-signal and complex environments.

3. 3D Point Cloud Modeling and Obstacle Localization

The point cloud modeling and localization method proposed in this section significantly enhances the accuracy of obstacle 3D geometric structure recognition and spatial positioning. Compared to traditional perspective projection methods, it reduces cumulative structural errors. When integrated with the high-precision BeiDou positioning results presented herein, it forms a "coordinate-level positioning + geometric-level recognition" capability for precise distribution network inspection perception [11,12]. The experimental section will subsequently validate that positioning errors are controlled within the 5 cm range, making it suitable for complex forest areas and overhead pole/tower scenarios.

To achieve precise spatial localization of obstacles (such as tree obstructions, external debris, and foreign objects entangled in power lines) during transmission and distribution line inspections, this paper constructs a three-dimensional point cloud environmental model based on drone-mounted LiDAR [13, 14]. It proposes a point cloud mapping and obstacle localization algorithm utilizing clustering and graph embedding techniques. The algorithm flow is illustrated in Figure 2.

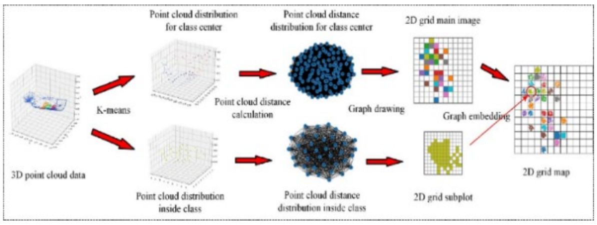

Figure 2. 3D Point Cloud Modeling and Obstacle Localization Workflow

First, the three-dimensional point cloud data collected by LiDAR can be represented as:

$$P = p_i = (x_i, y_i, z_i) \mid i = 1,2, \ldots, N \quad (6)$$

Where N represents the number of points. To distinguish different spatial structural regions within the inspection environment, the K-means algorithm is employed to perform point cloud clustering. The clustering objective function is defined as:

$$J = \sum_{i=1}^{k} \sum_{p_j \in C_i} \left|p_j - \mu_i\right|^2 \quad (7)$$

where (k) denotes the number of clusters, and μ_i represents the center of the i-th cluster.

After clustering is completed, Euclidean distances are calculated among points within each point cloud cluster to construct a spatial association map:

$$d_{ij} = \left|p_i - p_j\right|2 = \sqrt{(x_i - x_j)^2 + (y_i - y_j)^2 + (z_i - z_j)^2} \quad (8)$$

Constructing an undirected weighted graph based on the distance matrix:

$$G = (V, E, W) \quad (9)$$

Where V denotes the vertex set, (E) denotes the edge set, and (W) denotes the weight matrix, defined as:

$$w_{ij} = \begin{cases} e^{-d_{ij}^2/\sigma^2}, d_{ij} < r \\ 0, \text{otherwise} \end{cases} \quad (10)$$

Subsequently, the 3D point cloud map is embedded into a 2D is potential space using the optimal graph embedding function:

$$Y = \arg Y = \arg \min_{Y} \sum_{(i,j)} w_{ij} \left| y_i - y_j \right|^2 \quad (11)$$

Where (Y) represents the coordinates of a two-dimensional point cloud, solved using Laplacian Eigenmaps:

$$LY = \lambda DY \quad (12)$$

Laplacian Eigenmaps are adopted for graph embedding due to their ability to preserve local neighborhood and structural relationships within point cloud data, which is essential for accurate spatial reconstruction and obstacle localization. Compared with PCA, which primarily preserves global variance and may overlook local geometric structures, and t-SNE, which is mainly designed for visualization and has higher computational complexity, Laplacian Eigenmaps provide a more suitable representation for maintaining spatial connectivity and geometric consistency in transmission and distribution network inspection environments.
The point cloud is ultimately mapped onto a two-dimensional grid plane to construct a grid distribution image:

$$M(u, v) = f(Y_i) \quad (13)$$

This mapping structure is used to divide the environmental point cloud into a main grid map (global environment) and sub-grid maps (local obstacle regions), generating a two-dimensional obstacle grid map to enable UAV path planning and obstacle avoidance control. The formula for estimating the center position of an obstacle is:

$$P_{obs} = \frac{1}{|C_{obs}|} \sum_{p_i \in C_{obs}} p_i \quad (14)$$

To enhance obstacle perception, the semantic interpretation of clustered point clouds is used to distinguish environmental elements. Vegetation is identified as dense irregular clusters, conductors as elongated linear structures, and suspended debris as sparse isolated clusters. This improves separation accuracy and interpretability in complex transmission and distribution environments.

UAV inspection images are first processed by the improved YOLOv8n model to detect components and obstacles through bounding box outputs. The detected regions are then associated with LiDAR point cloud and BeiDou positioning data through spatial mapping and coordinate transformation, enabling the conversion of detection outputs into spatial coordinates for precise obstacle localization and improved workflow interpretability.
To enhance system completeness, detected faults and reconstructed 3D coordinates are converted into operational outputs for UAV control. Fault detections from the improved YOLOv8n model trigger maintenance alarm signals transmitted via the BeiDou link, while 3D coordinates from LiDAR reconstruction are used to update navigation maps and enable autonomous flight path adjustment. This ensures closed-loop decision-making for real-time fault reporting and UAV navigation.

4. Target detection algorithms

Target detection is one of the three core jobs in the science of computer vision. It involves identifying the type of target item in the image as well as calibrating its position to achieve the goals of localization and category determination [15,16]. Regression-based target detection methods employ convolutional neural networks to directly predict the category and location of targets, resulting in improved real-time performance. In particular, the YOLOv5 network can adapt to the anchor frame, which provides better detection for small targets. In addition, the model of YOLOv5 is easy to deploy, which is more suitable for the detection of safety hazards in complex construction scenarios [17].
The input side (Input layer), the backbone network (Backbone layer), the image feature combination layer (Neck layer), and the prediction side (Prediction layer) are the YOLOv5 network model's four main constituents. Figure 3 shows the overall topology of the network.

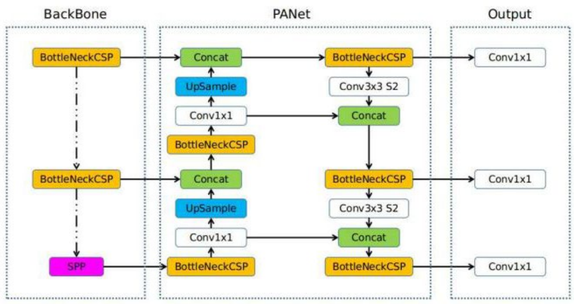

Figure 3. YOLOv5 Network Structure Diagram

(1) Input layer: The three input components of YOLOv5 are adaptive picture scaling, mosaic data enhancement, and adaptive optimal anchor frame computation. In contrast to other techniques, YOLOv5 can calculate the scaling ratio to determine the scaled image's size and the black border

padding value to add the black border to the original image adaptively without introducing too many parameters that would slow down the inference process. preventing an excessive number of parameters from impacting the inference speed. The Mosaic data augmentation method improves the precision of small target recognition by utilising dynamic scaling and cropping techniques. Also, in the initial anchor frame setting, YOLOv5 uses adaptive computation to obtain initial values. Then, iterating to optimise the prediction results, it outputs prediction frames, compares them with real frames, calculates errors, and updates the network parameters via back propagation.

(2) Backbone Layer: The Focus and CSPNet (Cross Stage Partial Networks) structures make up the backbone of YOLOv5.In YOLOv5, a new structure called the Focus structure makes greater use of the slicing function. Utilising the YOLOv5s structure as an illustration, the Focus structure receives the 608×608×3 original picture as input. A 304×304×12 feature map is produced after the slicing process, and a 304×304×32 feature map is produced after the convolution operation using 32 convolutional kernels. This effectively lowers the computational complexity and memory consumption, thereby increasing the model's operating speed. This process can efficiently lower memory usage and computational complexity, increasing the model's operating speed. Moreover, CSP1_X and CSP2_X, two CSP structures created by YOLOv5, are based on the CSP structure found in the YOLOv4 backbone network. Applying the CSP1_X structure mainly to the Backbone network and the CSP2_X structure largely to the Neck structure improves the characterization ability and operation efficiency of the model.

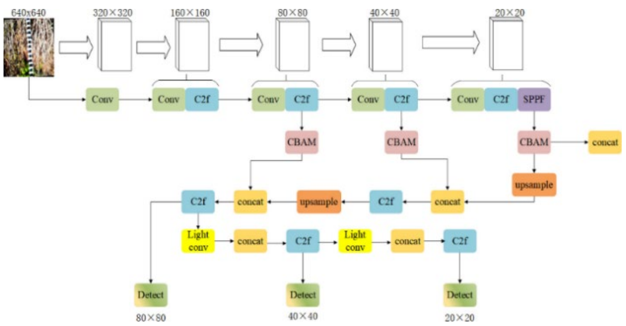

Figure 4. Optimization of the Structure Enhancement and Feature Extraction Module

As shown in Figure 4, to further enhance detection performance for small and densely clustered targets such as tree obstructions, foreign objects on wires, and bird nests in distribution network inspection scenarios, this paper optimizes the structural enhancement and feature extraction modules based on the YOLO backbone architecture. Figure 4 illustrates the improved YOLO model structure proposed in this paper. The model primarily consists of an input stage, backbone network, feature fusion layer (Neck), and detection stage (Head). It also incorporates lightweight convolution modules (Light Conv) and attention mechanism modules (CBAM) to enhance object recognition capabilities under complex background conditions.

In the backbone section, a C2f structure replaces the traditional C3 module to enhance cross-layer information flow and feature representation capabilities. Combined with the SPPF (Spatial Pyramid Pooling Fast) module, it aggregates global receptive fields through multi-scale pooling to improve structural shape feature extraction. The output features from this section can be represented as:

$$F_b = \mathrm{SPPF}(\mathrm{C2f}(X)) \tag{15}$$

where X denotes the input image features, and F_b denotes the backbone structure output.

The Neck layer employs a hybrid FPN-PAN architecture for multi-scale feature fusion, with a Convolutional Block Attention Module (CBAM) embedded in the main path to enhance the representation of key region information. The CBAM attention mechanism is defined separately for the channel and spatial mappings as follows:

$$M_c(F) = \sigma(\mathrm{MLP}(\mathrm{AvgPool}(F)) + \mathrm{MLP}(\mathrm{MaxPool}(F))) \tag{16}$$

$$M_s(F) = \sigma(\mathrm{Conv}([\mathrm{AvgPool}(F); \mathrm{MaxPool}(F)])) \tag{17}$$

The final fusion feature can be defined as:

$$F' = M_s(M_c(F)) \otimes F \tag{18}$$

Additionally, to reduce the computational burden of large-scale point cloud image processing and real-time detection, this paper introduces a lightweight convolution (Light Conv) module. Employing separable convolutions, it reduces both the number of parameters and computational overhead. The computational complexity comparison can be expressed as:

$$\mathrm{FLOPs}dw = k^2 \cdot Cin \cdot H \cdot W + C_{in}C_{out} \cdot H \cdot W \tag{19}$$

Compared to standard convolutions:

$$\mathrm{FLOPs}std = k^2 \cdot CinC_{out} \cdot H \cdot W \tag{20}$$

Achieve a significant structural compression ratio:

$$R = \frac{\mathrm{FLOPs}dw}{\mathrm{FLOPs}std} \ll 1 \tag{21}$$

Ultimately, the backbone output features undergo upsampling and multi-scale fusion to generate feature maps at scales of (80 × 80), (40 × 40), and (20 × 20) for detecting objects of corresponding sizes, thereby enhancing the recognition and resolution capabilities for small-scale features.

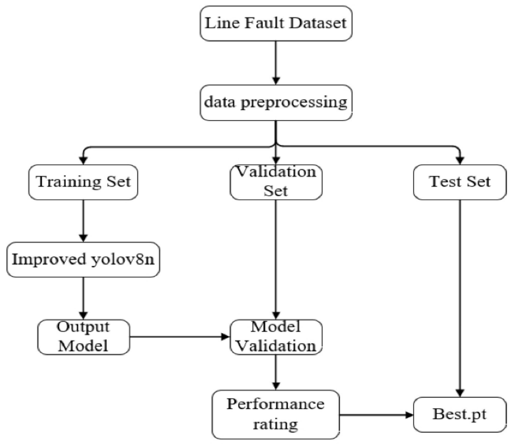

Figure 5. Algorithm Flowchart

Figure 5 illustrates the training and validation process of the improved YOLOv8n model for identifying faults and obstacles on power transmission and distribution lines. First, fault data collected from transmission lines via drone inspections undergoes standardized preprocessing, including image cleaning, sample balancing, and data augmentation, to enhance the model's adaptability to complex power inspection scenarios. Following preprocessing, the dataset is proportionally divided into training, validation, and test sets. The training set drives feature learning in the improved YOLOv8n model, while the validation set evaluates and tunes model performance during training to ensure a reasonable balance between detection accuracy and inference efficiency. During the training phase, the improved model iteratively updates its parameters based on the training dataset. After each training cycle, the model's performance is validated using the validation set to ensure it can effectively recognize small targets, densely packed targets, and target features in complex backgrounds. When the model achieves optimal performance on the validation set, its output is selected as the candidate weight file. Subsequently, the candidate model undergoes final performance evaluation using an independent test set to assess its generalization capability and real-world application performance. Based on the evaluation results, the best-performing model weight file, Best.pt, is selected for subsequent deployment on the drone edge device and for defect identification tasks in actual power transmission and distribution inspection scenarios.

5. Experiments

A comparison experiment was created to confirm the usefulness of the transmission line tree barrier prediction model based on 3D imaging LiDAR technology.

5.1 Experimental environment

Based on the outcomes of each numerical record, the mean transit time and tree barrier voltage drop for the experimental group and the control group are computed. A transmission line is installed between the laser incidence pile and the laser outgoing pile, and the tree barrier structure is positioned at the designated location [18,19]. The real distance between each tree barrier organisation and the transmission line is then counted separately. Of these, the power host in the experimental group carries a novel kind of prediction model, whereas the power host in the control group carries a transmission fault prediction model of the point cloud type [20]. To make the tree fault prediction experiment easier to implement, the transmission line tree fault is configured as Figure. 6.

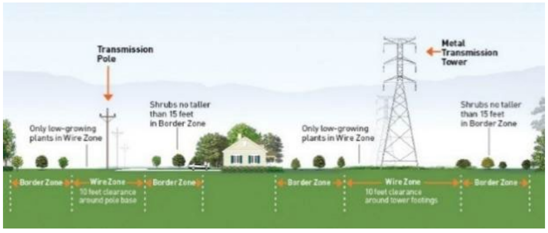

Figure 6. Transmission line tree barrier setup

Table 2. Category Distribution of the Transmission-Line Inspection Dataset

Category	Training	Validation	Testing	Total
Insulators	1,820	390	390	2,600
Icing Defects	1,610	345	345	2,300
Foreign-Object Hazards	1,750	375	375	2,500
Conductors	1,890	405	405	2,700
Total	**7,070**	**1,515**	**1,515**	**10,100**

Table 2 presents the category distribution of the transmission-line inspection dataset used for training and evaluating the improved YOLOv8n model. The dataset consists of four representative inspection categories, including insulators, icing defects, foreign-object hazards, and conductors. A train-validation-test split ratio of approximately 70:15:15 was adopted. The sample distribution remains relatively balanced across categories, reducing class imbalance effects and improving the reliability of model training and evaluation.

5.2 Analysis of results

When the incidence of electrons is equal to $1.0 \times 10^9 T$,$2.0 \times 10^9 T$,$3.0 \times 10^9 T$,$4.0 \times 10^9 T$,$5.0 \times 10^9 T$,$6.0 \times 10^9 T$,$7.0 \times 10^9 T$,$8.0 \times 10^9 T$,$9.0 \times 10^9 T$, As seen in Table 3, note the precise variations in the mean electron transfer durations of the experimental and control groups in this instance. Close all laser switches within the transmission line.

Table 3. Comparison of Mean Electron Transit Time (Unit: μs)

Electron incidence rate/($\times 10^9 T$)	Average mean transit cycle/ μ S		
	Experimental group (μs)	Control group (μs)	Ideal value (μs)
1.0	0.39	0.88	0.62
2.0	0.34	0.88	0.64
3.0	0.30	0.88	0.64
4.0	0.29	0.86	0.64
5.0	0.27	0.91	0.55
6.0	0.25	0.91	0.55
7.0	0.56	0.95	0.58
8.0	0.26	0.94	0.50
9.0	0.22	0.94	0.51

Table 3 analysis reveals that, in the optimum state, the mean transit time begins to continually decline when the incident electron amount exceeds 6.0×109T, although it always stays at 0.63 μs before it reaches 5.0×109T. The mean transit time for the experimental group has been decreasing before the amount of incident electrons reaches 4.0×109T. It stabilized temporarily before decreasing again, with the early-stage reduction significantly larger than the late-stage reduction, reaching a maximum of only 0.40 μs. For the control group, the mean transit time remained stable until the incident electron amount reached 4.0×109T. The electron transport period starts to rise continuously when the incident electron amount reaches 5.0×109T, and the global maximum value reaches 0.97 μs, which is 0.57 μs less than the extreme value of the experimental group.In summary, it is evident that the new type of tree-barrier prediction model can be used to effectively predict electronic tree barriers while keeping the actual prediction distance constant, provided that the new model is applied and the average transmission period of electrons is shortened.

It is well known that the voltage differential drop across the tree barrier can be used to characterise the LiDAR host's ability to operate, maintain, and manage safely on the transmission line. Generally speaking, the greater the voltage differential drop, the greater the management ability of the latter, and vice versa. Table 4 details the precise variations in voltage differential drop across the tree barrier in the experimental and control groups over the course of the 50-min experiment.

Table 4. Comparison of Voltage Differential Drop Across Tree Barrier

Experimental time /min	Tree barrier voltage drop value		
	Experimental group	Control group	Ldeal value
10	200.9	124.8	155.8
20	202.6	125.6	158.4
30	203.4	126.4	157.8

40	204.4	128.3	157.9
50	204.7	128.4	158.2

Table 4 analysis reveals that, in perfect conditions, the voltage differential drop across the tree barrier remains constant as the experimental duration increases. The tree barrier voltage drop represents the voltage attenuation caused by vegetation or tree canopies obstructing the transmission path. It reflects the level of signal or power degradation due to environmental obstacles. A higher voltage drop indicates stronger obstruction and reduced system performance, while a lower value suggests improved transmission conditions and better inspection efficiency. Therefore, this metric is directly related to the reliability of UAV-based inspection in complex distribution network environments.

The differential drop of the tree barrier voltage in the experimental group increases over the course of the experiment, reaching a worldwide maximum value of 204.7 V. The global maximum value only reaches 126.4 V, which is 77 V lower than the extreme value in the experimental group. The differential drop of the tree barrier voltage in the control group continues to rise during the first 30 minutes of the experiment, and it tends to stabilise after that. stays constant, the new tree-barrier prediction model results in a notable increase in the voltage differential drop across the tree barrier.

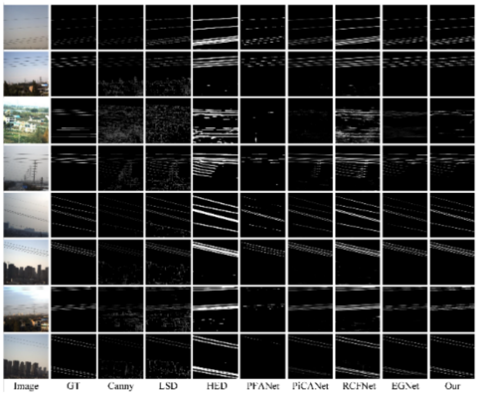

Figure 7. Visualization of Multiple Line Inspection Methods in Transmission and Distribution Patrol Scenarios

Figure 7 presents a visual comparison of various typical line detection and edge extraction methods applied to power transmission and distribution line scenarios, including Canny, LSD, HED, PFANet, PiCANet, RCFNet, EGNet, and the improved algorithm proposed in this paper. To validate the model's robustness in complex backgrounds, experiments selected representative distribution network inspection scenarios, including urban building backgrounds, dense tree obstructions, strong sky glare interference, low-illumination nighttime conditions, and large-scale power line overlaps. The GT column reveals the distribution of actual edge annotations. Traditional edge detection algorithms (e.g., Canny and LSD) exhibit significant shortcomings in areas with strong background noise or overlapping cables, resulting in severe false positives and false negatives. Deep learning-based methods like HED and RCFNet partially mitigate structural loss issues but still show noticeable discontinuities in weak edges and complex textures. Attention-driven networks (PFANet, PiCANet, and EGNet) enhance long, thin line structures but struggle to maintain complete boundaries under occlusion and extreme lighting variations. In contrast, the proposed model effectively extracts complete, continuous edge structures of transmission and distribution lines across diverse scenarios, significantly suppressing background noise interference. This results in a clear, continuous, and stable representation of power lines in the image, particularly demonstrating exceptional edge retention capabilities in densely populated multi-object regions and occlusion areas.

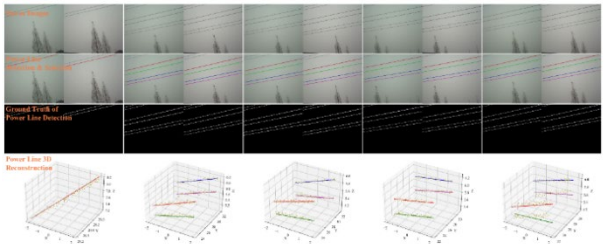

Figure 8. Visualization of Power Line Inspection and 3D Spatial Reconstruction Experiment

Figure 8 presents the experimental results of distribution and transmission line detection and 3D spatial reconstruction using the proposed improved YOLOv8n detection model and 3D point cloud reconstruction algorithm. The raw inspection image in the first row reveals that under foggy conditions, low contrast, and complex backgrounds, the visual edges of power lines become extremely blurred, making accurate identification challenging for traditional image detection methods. The second row displays detection results after our model identifies and performs pixel-level parsing of power lines. The model accurately extracts multiple line structures despite fog, occlusions, and uneven brightness, maintaining line continuity and edge integrity. This significantly outperforms traditional visual methods and the unmodified YOLO model. The third row presents Ground Truth results showing manually annotated actual line boundaries. It is evident that our method achieves high consistency with the true results in terms of positioning accuracy and geometric consistency for multiple target lines. The bottom section demonstrates the 3D power line reconstruction process based on detection results and the final spatial restoration effect. Through point cloud and coordinate transformation techniques, it achieves precise spatial position recovery and 3D geometric structure fitting for multiple transmission lines.

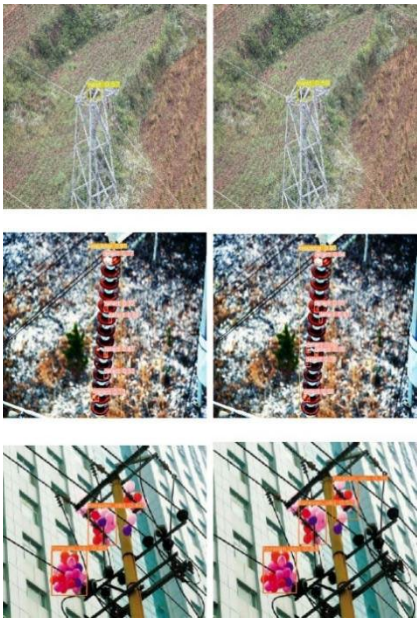

Figure 9. Fault Identification in a Typical Transmission and Distribution Inspection Scenario

Figure 9 demonstrates the typical defect recognition results for power transmission and distribution lines achieved by the proposed model based on an improved YOLOv8n framework, covering inspection scenarios such as tower structure recognition, insulator flashover detection, and foreign object detection. The figure demonstrates that our model maintains high target localization accuracy and structural integrity even under complex background textures, cluttered tree obstructions, and strong mixed illumination interference. Compared to the unmodified model, our approach exhibits superior detection consistency and stability in edge regions and small target locations. Detection boxes more accurately align with target contours, effectively mitigating issues such as edge discontinuity, misdetection, and missed objects. Particularly in scenarios involving slender insulator strings and foreign object hanging, traditional detection networks often produce significant false positives due to scale imbalance and insufficient feature representation. The introduced CBAM attention mechanism and lightweight convolutional modules significantly enhance the network's sensitivity to critical structural features, yielding more refined and reliable detection results.

(a)

(b)

Figure 10. Detection in Scenarios of Insulator Icing Faults and Foreign Object Entanglement on Power Lines

Figure 10 demonstrates the detection performance of the improved YOLOv8n model proposed in this paper for identifying defects in critical components of power transmission and distribution lines, covering two typical safety risk scenarios: insulator icing faults and foreign objects entangled in lines. Figure (a) illustrates the identification of pin-type insulators under varying degrees of icing. It can be observed that even under complex conditions—such as severe ice coverage obscuring surface textures, background grayscale values approaching target structures, and narrow spacing between insulators—the model accurately locates insulator regions and achieves stable classification. The recognition results maintain high confidence levels, demonstrating excellent detection continuity and structural integrity even around elongated structures with fractured edges and under severe noise interference. This indicates that the proposed attention enhancement mechanism effectively improves key feature expression capabilities, enabling the model to accurately extract weakly textured targets. Figure (b) demonstrates the model's capability to identify foreign objects hanging on conductors during drone inspections. The model successfully detected plastic bag-like debris suspended above the wires, outputting clear detection bounding boxes and confidence labels. This further proves that the proposed model can effectively locate high-risk obstacles prone to causing arcing or wire breakage incidents during practical inspections.

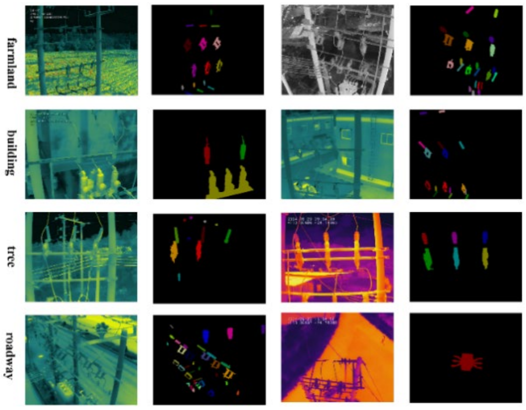

Figure 11. Visualization of Target Detection for Transmission and Distribution Line Patrols in Different Environmental Scenarios

Figure 11 demonstrates the target detection visualization results of the improved YOLOv8n model proposed in this paper across diverse distribution network inspection scenarios, including typical complex backgrounds such as farmland, building areas, forested environments, and roadways. Experimental results demonstrate that under varying scene conditions, target density, and category distributions, the model accurately identifies critical transmission and distribution line components (insulators, fittings, conductors, and auxiliary structures) alongside potential safety hazard targets. It maintains robust spatial separation and stable detection continuity. In farmland and forest scenarios, traditional models often suffer from false positives or false negatives due to vegetation occlusion, complex background textures, and targets with colors similar to the background. The proposed method enhances feature expression capabilities for critical structures through the CBAM attention mechanism and lightweight feature fusion module, enabling accurate target extraction in challenging environments.

Table 5. Comparison of Reconstruction Performance with ICP and SLAM-Based Mapping Methods

Method	Obstacle Localization RMSE (cm)	Chamfer Distance	Reconstruction Time (s)	Mapping Accuracy (%)
ICP	5.8	0.038	2.45	91.6
ORB-SLAM2	4.9	0.032	2.12	93.4
RTAB-Map SLAM	4.3	0.029	1.96	94.2
K-means + Laplacian Eigenmaps	2.7	0.016	1.31	97.3

Table 5 compares the proposed K-means + Laplacian Eigenmaps reconstruction pipeline with ICP and SLAM-based mapping approaches. The proposed method achieves the lowest obstacle localization RMSE (2.7 cm) and Chamfer Distance (0.016), indicating superior spatial precision. It also provides the fastest reconstruction time (1.31 s) and the highest mapping accuracy (97.3%), demonstrating its effectiveness for accurate and efficient transmission-line inspection and obstacle localization.

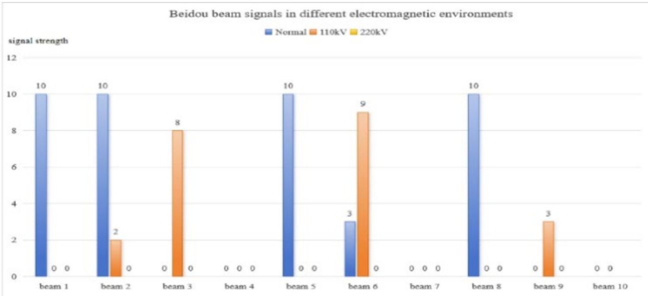

Figure 12. Measurement of BeiDou Satellite Beam Signal Strength Under Different Electromagnetic Interference Environments

Figure 12 illustrates the variation in BeiDou satellite beam signal strength under different electromagnetic environments, including interference-free normal conditions, 110 kV distribution network lines, and 220 kV high-voltage transmission lines. Ten representative BeiDou beams were selected for signal strength measurements to evaluate the stability and availability of BeiDou communication links under strong electromagnetic interference conditions. Results indicate that in the normal environment, all beam signal strengths maintained high values around 10, demonstrating stable and reliable communication quality. However, in the 110 kV distribution network environment, most beams exhibited varying degrees of attenuation, with beams 2, 6, and 9 showing the most pronounced drops to 2, 3, and 3, respectively, indicating the distribution network's electric field significantly impacted certain satellite-to-ground links. Under 220 kV high-voltage transmission conditions, signal attenuation became more pronounced, with nearly all beams experiencing severe reductions or near-loss, and multiple beams dropping to zero intensity. This demonstrates that conventional communication methods are highly susceptible to link disruption under conditions of strong electromagnetic coupling. These experimental results directly validate the importance of deploying BeiDou short message communication in high-intensity electromagnetic interference zones, as proposed in this paper. They also corroborate the practical engineering value of the designed "BeiDou + edge computing" communication model in ensuring the stability of UAV inspection missions.

Table 6. Robustness Evaluation of the Proposed YOLOv8n Model under Challenging Environmental Conditions

Environment	**Precision (%)**	**Recall (%)**	**F1-score (%)**	**mAP50 (%)**
Normal	93.2	92.6	92.9	94.1
Fog	91.4	90.7	91	91.8
Glare	90.7	89.9	90.3	90.9
Nighttime	89.8	88.6	89.2	89.7
Occlusion	90.2	89.4	89.8	90.4
Rainy	90.9	90.1	90.5	91.2

Table 6 presents the robustness evaluation of the proposed YOLOv8n model under various challenging environmental conditions. Although detection performance decreases slightly under fog, glare, nighttime, occlusion, and rainy scenarios, the model consistently maintains high Precision, Recall, F1-score, and mAP50 values. These results demonstrate the strong robustness and reliability of the proposed visual recognition framework for UAV-based transmission-line inspection in complex real-world environments.

Table 7. BeiDou RDSS Communication Performance under Electromagnetic and Weak-Signal Environments

Environment	**Throughput (kbps)**	**Retransmission Burden (%)**	**Packet Arrival Consistency (%)**	**Average Delay (ms)**
Normal	42.6	1.1	99.6	38.4
110 kV Electromagnetic Interference	39.8	2.3	98.8	45.7
220 kV Electromagnetic Interference	36.4	4.7	97.5	57.9
Mountain Forest Weak Signal	35.7	5.1	97.1	61.3
Severe Electromagnetic Environment	33.9	6.4	96.2	69.8

Table 7 presents the communication performance of the BeiDou RDSS system under different environmental conditions. Although throughput decreases and delay increases with stronger electromagnetic interference, the system maintains a packet arrival consistency above 96% in all scenarios. Even under severe electromagnetic conditions, the retransmission burden remains below 7%, demonstrating the robustness and reliability of the proposed communication framework for UAV-based transmission-line inspection.

Table 8. Patrol-Oriented Performance Evaluation of the Proposed BeiDou Edge-YOLO Inspection Framework

Metric	**Unit**	**Baseline System**	**Proposed BeiDou Edge-YOLO System**
Detection Latency	ms	46.8	28.6
Communication Success Ratio	%	94.2	98.7
Obstacle Ranging Deviation	cm	6.4	2.8
Route Inspection Efficiency	%	87.5	95.6
Patrol Alarm Response Time	s	3.8	2.1
Inspection Coverage	%	89.1	96.8

Table 8 presents the patrol-oriented performance evaluation of the proposed BeiDou Edge-YOLO framework. Compared with the baseline system, the proposed approach reduces detection latency from 46.8 ms to 28.6 ms and obstacle ranging deviation from 6.4 cm to 2.8 cm, while improving the communication success ratio from 94.2% to 98.7% and route inspection efficiency from 87.5% to 95.6%. The framework also achieves faster alarm response and higher inspection coverage, demonstrating its effectiveness for real-time UAV-based transmission-line inspection.

Table 9. Ablation Study of Individual and Combined YOLOv8n Enhancement Modules

Model Configuration	C2f	CBAM	Light Conv	Precision (%)	Recall (%)	F1-score (%)	mAP50 (%)
YOLOv8n Baseline	No	No	No	88.3	87.5	87.9	88.7
YOLOv8n + C2f	Yes	No	No	90.1	89.2	89.6	90.6
YOLOv8n + CBAM	No	Yes	No	90.5	89.7	90.1	91.1
YOLOv8n + Light Conv	No	No	Yes	89.6	88.9	89.2	89.8
YOLOv8n + C2f + CBAM	Yes	Yes	No	92.1	91.4	91.7	92.6
Proposed YOLOv8n + C2f + CBAM + Light Conv	Yes	Yes	Yes	93.2	92.6	92.9	94.1

Table 9 presents the ablation study results of the proposed YOLOv8n model. The C2f, CBAM, and Light Conv modules baseline YOLOv8n. The mAP50 increases from 88.7% (baseline) to 90.6%, 91.1%, and 89.8% after introducing C2f, CBAM, and Light Conv, respectively. Combining C2f and CBAM further improves mAP50 to 92.6%. The complete model integrating all three modules achieves the best performance, with 93.2% Precision, 92.6% Recall, 92.9% F1-score, and 94.1% mAP50, demonstrating the effectiveness of the proposed architecture.

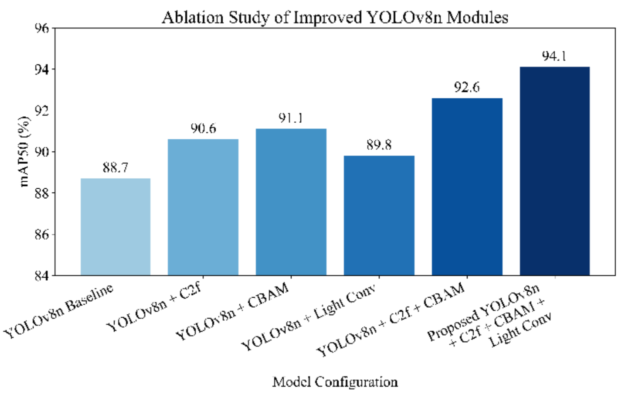

Figure 13. Ablation Study of Improved YOLOv8n Modules for Distribution Network Inspection

Figure 13 illustrates the impact of individual and combined YOLOv8n enhancements on detection performance. Among the individual modules, CBAM achieves the largest improvement in mAP50, followed by C2f, while Light Conv provides a moderate accuracy gain with reduced computational complexity. The complete model integrating C2f, CBAM, and Light Conv achieves the highest mAP50 of 94.1%, demonstrating the effectiveness of the proposed architecture.

Table 10. Computational Complexity Comparison of Baseline and Proposed YOLO Models

Model	Parameters (M)	FLOPs (G)	Model Size (MB)	Inference Time (ms)	FPS
YOLOv5n	1.9	4.5	3.9	14.8	67.5
YOLOv8n Baseline	3.21	8.7	6.3	11.4	87.7
YOLOv8s	11.2	28.6	21.5	24.5	40.8
Proposed YOLOv8n	2.74	6.95	5.35	8.9	112.4

Table 10 compares the computational complexity of the proposed YOLOv8n model with representative YOLO variants. The proposed model achieves lower computational cost than the baseline YOLOv8n, reducing the number of parameters from 3.21 M to 2.74 M and FLOPs from 8.70 G to 6.95 G. In addition, the model size decreases from 6.3 MB to 5.35 MB, while the inference time is reduced from 11.4 ms to 8.9 ms. The FPS increases from 87.7 to 112.4, demonstrating improved real-time processing capability and deployment efficiency for UAV-based edge computing applications.

Table 11. Onboard Deployment Performance of the Proposed YOLOv8n Model on Edge Devices

Edge Device	FPS	Inference Time (ms)	Memory Occupancy (MB)	Energy Demand (W)
Jetson Nano	28.4	35.2	1285	8.7
Jetson Xavier NX	65.7	15.2	1740	13.6
Jetson Orin Nano	91.3	10.9	2135	18.9

RK3588	52.6	19	1390	9.8

Table 11 presents the onboard deployment performance of the proposed YOLOv8n model across representative edge-computing platforms. The results show that the model achieves real-time inference on all tested devices, with FPS ranging from 28.4 to 91.3 and inference times between 10.9 ms and 35.2 ms. The memory occupancy and energy demand remain within the capabilities of embedded edge hardware, demonstrating the suitability of the proposed model for practical UAV-based transmission-line inspection and BeiDou edge-computing applications.

The proposed edge computing framework is designed to support efficient UAV-based deployment under practical resource constraints. The model incorporates lightweight architectural improvements, including optimized convolutional operations and reduced feature redundancy, to minimize memory consumption and computational overhead. These design strategies enable stable real-time inference on onboard UAV edge devices while maintaining high detection performance. The system is therefore suitable for continuous operation in transmission and distribution line inspection tasks under complex environmental and hardware-limited conditions. Furthermore, the distributed edge-computing architecture supports coordinated operation of multiple UAVs, enabling efficient inspection of geographically extensive transmission and distribution networks. By performing local data processing and transmitting only critical inspection results through the BeiDou communication link, the framework reduces network load while maintaining reliable large-scale inspection coverage and real-time operational responsiveness.

6. Conclusion

This paper addresses critical challenges in existing transmission and distribution line inspections—including low target recognition accuracy, insufficient communication reliability, and lack of three-dimensional spatial understanding—by proposing an intelligent drone-based distribution network inspection technology system that integrates BeiDou satellite communication with edge computing. By constructing an enhanced YOLOv8n detection network, the system significantly improves recognition capabilities for slender structures and small targets in complex backgrounds. Techniques such as point cloud clustering and graph embedding enable high-precision reconstruction of transmission line three-dimensional geometric structures, providing reliable spatial positioning support. The BeiDou short message link enhances data transmission capabilities in unstable regions, effectively resolving the issue of real-time data transmission failure in high-voltage electromagnetic environments and communication blind spots. Comprehensive experimental validation demonstrates that the proposed method achieves significant optimization in recognition accuracy, real-time performance, and anti-interference capability, exhibiting excellent scalability and deployment value for practical engineering applications. The proposed system has strong implementation potential for practical power grid inspection applications. Its lightweight design and compatibility with UAV platforms enable efficient deployment in real-world transmission and distribution networks. The framework supports automated inspection, fault detection, and operational maintenance in complex environments.

Future work will investigate transformer-based detection architectures to enhance global context modeling and improve robustness in complex inspection environments. In addition, advanced multi-modal fusion strategies will be explored to effectively integrate visual imagery, LiDAR point clouds, and BeiDou positioning data, enabling more comprehensive environmental perception and improved decision-making capability in UAV-based inspection systems. Future work will further advance visual and multi-sensor fusion positioning technologies, explore sequential spatio-temporal feature learning to enable path risk prediction and autonomous decision-making, and investigate model compression methods to enhance edge computing capabilities for drones. This will drive progress toward fully intelligent inspection workflows and multi-drone collaborative operations.

Declarations Funding

Fund Project: Vehicle mounted Intelligent Distribution Network Inspection Technology Based on Beidou+AI (Supported by State Grid Zhejiang Electric Power Co., Ltd. Science and Technology Project (Project Number: 521156250001))

Conflict of Interest

The authors declare that they have no conflicts of interest regarding this work.

Data Availability

The data that support the findings of this study are not publicly available due to confidentiality agreements but are available from the corresponding author upon reasonable request.

Code Availability

Not applicable.

Author Contributions

Ying Xie: Conceptualization, Methodology, Formal analysis, Writing – original draft, Supervision.
Yi Jiang: Data curation, Investigation, Writing – review & editing.
Lichao Cui: Software, Visualization, Validation.
Yongjian Zhang: Resources, Project administration, Funding acquisition.
Jiangning Zhao: Conceptualization, Methodology, Writing – review & editing.

References

[1] M. A. Berwo, A. Khan, Y. Fang, H. Fahim, S. Javaid, J. Mahmood, and S. MS, "Deep learning techniques for vehicle detection and classification from images/videos: A survey," *Sensors*, vol. 23, no. 10, p. 4832, 2023, https://doi.org/10.3390/s23104832

[2] S. Li, G. Liu, L. Li, Z. Zhang, W. Fei, and H. Xiang, "A review on air-ground coordination in mobile edge computing: Key technologies, applications and future directions," *Tsinghua Science and Technology*, vol. 30, no. 3, pp. 1359–1386, 2024, https://doi.org/10.26599/TST.2024.9010142

[3] A. Sanaeifar, M. L. Guindo, A. Bakhshipour, H. Fazayeli, X. Li, and C. Yang, "Advancing precision agriculture: The potential of deep learning for cereal plant head detection," *Computers and Electronics in Agriculture*, vol. 209, p. 107875, 2023, https://doi.org/10.1016/j.compag.2023.107875

[4] C. Zhang, G. Shan, and B.-H. Roh, "Fair federated learning for multi-task 6G NWDAF network anomaly detection," *IEEE Trans. Intell. Transp. Syst.*, vol. 26, no. 10, pp. 17359–17370, 2025, https://doi.org/10.1109/TITS.2024.3461679

[5] H. Liang, S. C. Lee, W. Bae, J. Kim, and S. Seo, "Towards UAVs in construction: Advancements, challenges, and future directions for monitoring and inspection," *Drones*, vol. 7, no. 3, p. 202, 2023, https://doi.org/10.3390/drones7030202

[6] G. Ding, H. Fu, and J. Li, "Research and application of Power 5G communication device for distributed power sources and active distribution networks," in *Proc. 4th Int. Conf. Neural Netw., Inf. Commun. Eng. (NNICE)*, 2024, pp. 1145–1149, http://doi.org/10.1109/NNICE61279.2024.10498842

[7] H. Liang, T. Lin, and X. Lin, "Research on AI-based digital image detection of road surface damage for autonomous driving," in *Proc. SPIE Int. Conf. Signal Image Process. Commun. (ICSIPC)*, vol. 13800, pp. 240–246, 2025. https://doi.org/10.1117/12.3077011

[8] L. Xu, S. Dong, H. Wei, Q. Ren, J. Huang, and J. Liu, "Defect signal intelligent recognition of weld radiographs based on YOLO V5-improvement," *Journal of Manufacturing Processes*, vol. 99, pp. 373–381, 2023, http://doi.org/10.1016/j.jmapro.2023.05.058

[9] Q. Chen, Z. Guo, W. Meng, S. Han, C. Li, and T. Q. Quek, "A survey on resource management in joint communication and computing-embedded SAGIN," *IEEE Commun. Surv. Tutorials*, vol. 27, no. 3, pp. 1911–1954, 2024, http://doi.org/10.1109/COMST.2024.3421523

[10] Y. Han, Y. Fang, Y. He, Z. Liu, Z. Chen, L. Wang, and H. Shen, "Unmanned systems for wind power inspection and maintenance from onshore to offshore: A comprehensive review," *Nondestructive Testing and Evaluation*, pp. 1–46, 2025, https://doi.org/10.1080/10589759.2025.2587783

[11] D. Perikleous, G. Koustas, S. Velanas, K. Margariti, P. Velanas, and D. Gonzalez-Aguilera, "A novel drone design based on a reconfigurable unmanned aerial vehicle for wildfire management," *Drones*, vol. 8, no. 5, p. 203, 2024, https://doi.org/10.3390/drones8050203

[12] J. Liu, R. Jia, W. Li, F. Ma, H. M. Abdullah, H. Ma, and M. A. Mohamed, "High precision detection algorithm based on improved RetinaNet for defect recognition of transmission lines," *Energy Reports*, vol. 6, pp. 2430–2440, 2020, https://doi.org/10.1016/j.egyr.2020.08.037

[13] X. Li, L. Zhang, J. Zhang, and J. Li, "Research and application of joint inspection technology for box type intelligent substations," in *Proc. Int. Conf. Adv. Electr. Eng. Comput. Appl. (AEECA)*, 2024, pp. 147–153 https://doi.org/10.1109/AEECA62331.2024.00034

[14] J. Tang, S. Lei, J. Liu, N. Lv, and H. Qi, "Dual-branch hyperspectral open-set classification with reconstruction–prototype fusion for satellite IoT perception," *Remote Sensing*, vol. 17, no. 22, p. 3722, 2025, https://doi.org/10.3390/rs17223722

[15] J. Luo and W. Dong, "Accurate positioning method of maritime search and rescue target based on binocular vision," *Signal, Image and Video Processing*, vol. 19, no. 4, p. 311, 2025, https://doi.org/10.1007/s11760-025-03912-3

[16] W. Han, G. Yang, S. Chen, K. Zhou, and X. Xu, "Research progress on intelligent operation and maintenance of bridges," *Journal of Traffic and Transportation Engineering (English Edition)*, vol. 11, no. 2, pp. 173–187, 2024, http://doi.org/10.1016/j.jtte.2023.07.010

[17] D. Li, M. Wang, H. Guo, and W. Jin, "On China's earth observation system: Mission, vision and application," *Geo-Spatial Information Science*, vol. 28, no. 2, pp. 303–321, 2025, https://doi.org/10.1080/10095020.2024.2328100

[18] F. Wang, W. Sun, S. Lv, R. Zhang, L. Zhang, and S. Chen, "Research on the application of UAV intelligent patrol inspection technology in photovoltaic construction management," in *Digitalization and Management Innovation III*, IOS Press, 2025, pp. 693–700.

[19] X. Liang, W. Cheng, C. Zhang, L. Wang, X. Yan, and Q. Chen, "YOLOD: A task decoupled network based on YOLOv5," *IEEE Trans. Consumer Electron.*, 2023, http://doi.org/10.1109/TCE.2023.3278264

[20] Z. H. Khan, J. Zhang, and P. Zeng, "Proceedings of the Fourth International Conference on Mechanical, Electronics, Electrical and Automation Control (METMS 2024)," in *Proc. SPIE*, vol. 13163, 2024